4D Biofabrication of T-Shaped Vascular Bifurcation

Waseem Kitana, Indra Apsite, Jonas Hazur, Aldo R. Boccaccini, and Leonid Ionov*

4D Biofabrication – a pioneering biofabrication technique – involves the automated fabrication of 3D constructs that are dynamic and show shape-transformation capability. Although current 4D biofabrication methods are highly promising for the fabrication of vascular elements such as tubes, the fabrication of tubular junctions is still highly challenging. Here, for the first time, a 4D biofabrication-based concept for the fabrication of a T-shaped vascular bifurcation using 3D printed shape-changing layers based on a mathematical model is reported. The formation of tubular structures with various diameters is achieved by precisely controlling the parameters (e.g. crosslinking time). Consequently, the 3D printed films show self-transformation into a T-junction upon immersion in water with a diameter of a few millimeters. Perfusion of the tubular T-junction with an aqueous medium simulating blood flow through vessels shows minimal leakages with a maximum flow velocity of 0.11 m s^{-1}. Furthermore, human umbilical vein endothelial cells seeded on the inner surface of the plain T-junction show outstanding growth properties and excellent cell viability. The achieved diameters are comparable to the native blood vessels, which is still a challenge in 3D biofabrication. This approach paves the way for the fabrication of fully automatic self-actuated vascular bifurcations as vascular grafts.

1. Introduction

Cardiovascular diseases (CVDs), such as the coronary artery disease, are the primary cause of death globally, taking the lives of an estimated 17.9 million people each year.[1] For instance, about

W. Kitana, I. Apsite, L. Ionov
Faculty of Engineering Science
University of Bayreuth
Ludwig Thoma Straße 36A, 95447 Bayreuth, Germany
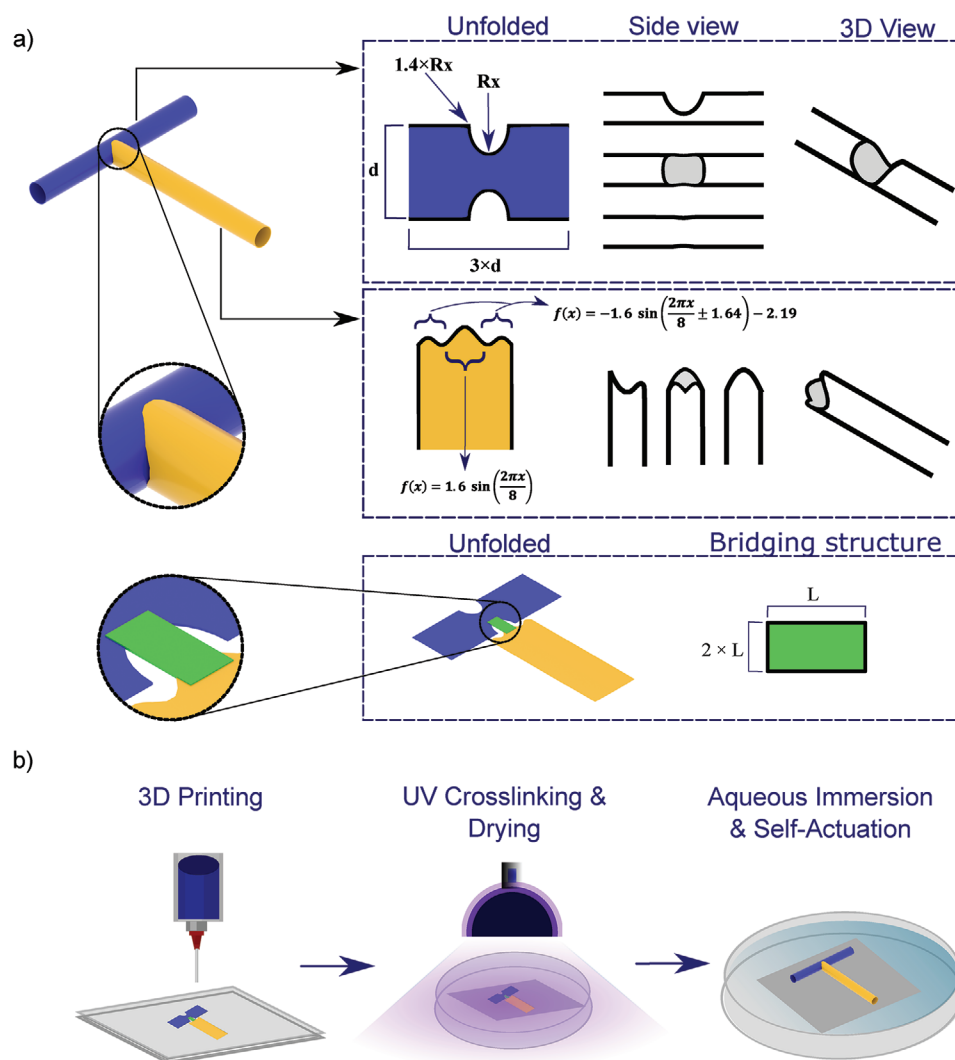E-mail: leonid.ionov@uni-bayreuth.de
J. Hazur, A. R. Boccaccini
Institute of Biomaterials
Department of Material Science and Engineering
Friedrich-Alexander-University Erlangen-Nuremberg
Cauerstr. 6, 91058 Erlangen, Germany
L. Ionov
Bavarian Polymer Institute
University of Bayreuth
Universitätsstraße 30, 95447 Bayreuth, Germany

half of the annual deaths in Europe alone are due to CVDs.[2] Further, it is anticipated that the annual global mortality rate of CVDs will increase up to 23.3 million by 2030.[3] Therefore, this requires urging advances in the strategies for the treatment and prevention of such diseases. Thus, the development of state-of-the-art blood vessel substitutes (synthetic vascular grafts) is highly demanded.

There is a wide range of treatment and prevention strategies for CVDs, spanning from food and lifestyle changing events to medications and medical procedures.[4,5] A clinical approach for treating such diseases is based on vascular grafts, which can be subdivided into autografts and artificial grafts.[4] Vascular autografts are the gold standard treatment method despite many shortcomings. One of the major shortcomings of the autograft-based approach is the limited availability.[4,6] Synthetic vascular grafts, which can be mass-produced and can solve the problem of the limited availability of autografts, show adequate clinical effectiveness in treating blood vessels of diameters > 6 mm.[4,6,7] However, small-diameter (Ø < 6 mm) synthetic vascular grafts have shown limited effectiveness. This is due to the low patency rates as well as restenosis for several reasons, such as the lack of cellular interactions upon transplantation.[6–10] In addition to that, the cell seeding on the inner surface of such grafts, which is crucial to prevent thrombus formation, is still a challenge.[11] Due to the significant drawbacks of synthetic vascular grafts and the limited availability of autologous vascular grafts, tissue engineering (TE) and biofabrication strategies have become promising alternatives to current approaches. Thus, the most advanced current strategies for the fabrication of vascular grafts are based on novel biofabrication techniques such as 3D (bio)-printing.[7,9,10,12]

The most commonly used techniques for the fabrication of tubular elements for vascular systems are 3D (bio)-printing,[13–15] projection stereolithography,[16,17] and electrospinning.[18–20] Despite the many advances in 3D biofabrication techniques, they still possess innate drawbacks towards the fabrication of vascular networks. These drawbacks may include; 1) the limited resolution for the application or deposition of cells,[7,21,22] 2) the need for support structures or sacrificial materials,[13,15] 3) the inability to produce intricate perfusable bifurcated vascular networks,[9] and 4) the 3D-biofabricated structures are usually static and do not interact with the surrounding biological environment.[12,23] Many of these challenges can be solved by using 4D (bio)-printing and, in a broader term, by 4D

**ADVANCED
SCIENCE NEWS**

www.advancedsciencenews.com

**ADVANCED
MATERIALS
TECHNOLOGIES**

www.advmattechnol.de

Figure 1. Schematic representation of the fabrication of T-junctions: a) the T-junction CAD design and b) the 4D biofabrication process.

biofabrication. 4D biofabrication is an emerging field, which is originally a 3D (bio)-printing technique combined with a fourth dimension (i.e., time) that allows the self-formation of tube-like structures with scalable diameters for tissue engineering vascular grafts (TEVGs).[12,24] According to the 4D biofabrication concept, the 3D printed structure transforms its shape over time by introducing external stimuli or responding to changes in the surroundings.[12,21,24] In this way, 4D biofabrication allows overcoming the above-mentioned limitations. This can be achieved by providing a dynamic environment for the fabrication of tubular constructs with a wide range of diameters. Moreover, these constructs mimic the complex native structure of tissues with high resolutions.[12,25] Further, it allows for simultaneous surface patterning of different cell types in a programmed way before initiating the folding process. As a result, it allows for the homogeneous seeding of cells on the inner surface of the tubular structure.[22,26] This results in a more homogeneous spreading and coverage of seeded cells. This shape-transformation property is caused by the inhomogeneous swelling of the overall structure, which can be due to

bilayer structure formation of a vertical gradient in crosslinking density/swelling degree (**Figure 1**b).[12,27,28] The 3D printing and photo-crosslinking of methacrylated alginate and hyaluronic acid solutions were recently used to fabricate tube-like structures.[12] These structures have tunable diameters and internal micro-architectures at high resolutions with a minimum average internal tube diameter of 20 µm.[12] In another approach, Zhang et al.,[6,25] proposed a 3D self-forming (4D biofabrication) microvascular scaffolds of different shapes (e.g., Y-bifurcation) based on gelatin methacrylamide (GelMA).[25] Although it demonstrated promising results as a vascular substitute, it shows loose or leaky tubular formations and cracks on the wall of the tubules, were observed. This leaky structure is formed due to that the hydrogel films were unbridged and had to be closed by increasing the extent of rolling of the self-formed microvessels.[25] Further, the resulted tubular shapes lack integrity and programmed bifurcation formation. Although 4D biofabrication has shown to be promising for fabricating relatively simple hollow structures such as spheres, 4D (bio)-printing/biofabrication of branched elements of vascular networks of

**ADVANCED
SCIENCE NEWS**

www.advancedsciencenews.com

**ADVANCED
MATERIALS
TECHNOLOGIES**

www.advmattechnol.de

small diameters is still a challenge. The essential element of tubular network formation is bifurcations, which can be realized, for instance, as T- or Y-shaped junctions. The fabrication of such bifurcations is challenging because of the presence of a gap between the perpendicularly connected tubes rolled from separate sheets (Figure S1, Supporting Information). Additionally, the rolling of singular sheets does not allow connecting tubular structures to form bifurcations (Figure S1, Supporting Information).

Herein, we propose a novel concept for the fabrication of vascular bifurcation substitute using a 4D biofabrication technique, in which a T-junction was chosen as a fabrication model. Hence, a complex CAD model with specific geometry was designed to achieve fully automated self-transformation of the hydrogel. Moreover, the formation of hydrogel-based tubular structures with diameters ranging from 2 to 15 mm with single and multiple rolls were achieved by precisely controlling the scale of the design, 3D printing parameters, rheological properties, and crosslinking time. Additionally, the perfusion of the T-junction with an aqueous solution showed minimal leakages with a maximum flow velocity of 0.11 m s^{-1}, which corresponds to an approximate volumetric flow rate of 0.78 mL s^{-1} in a 3 mm diameter of the fabricated bifurcated structure. The achieved flow rate is comparable with the flow rate of blood vessels of similar diameters.[29] Finally, human umbilical vein endothelial cells (HUVECs) attached to the inner surface of the tubular structure showed outstanding adhesion and growth properties along with excellent cell viability.

2. Results and Discussion

First, we developed a holistic approach to mathematically predict (i) the geometry of the initial sheets, (ii) to arrange them, and (iii) to fold them to yield T-shaped junctions of tubes of various diameters. These elements must allow the fabrication of vascular networks, which are also intrinsic to alveolar networks. In order to find out a proper geometry, which will form a T-junction upon shape transformation, we transferred the x, y, and z coordinates of points on the surface of complex folded 3D objects in x and y coordinates of the same sheets before folding (2D objects). The general strategy is based on the fact that folding results in the formation of tubular constructs, where the position of points can be easily described in radial coordinates (Figure S2, Supporting Information). The T-junction can be formed when two tubes merge – one tube crosses the other. The z coordinate of the crossing tube depends on the x coordinates as $z = R\sqrt{1 - x^2}$, where R is the radius of the tube. Meanwhile, the x coordinate can be described as $x = \cos t$, where t ranges from 0 to 2π. This yields $z = R\sqrt{1 - (\cos(t + \varphi))^2}$, where φ is the phase shift. The shape can be described as it is illustrated in Figure S2, Supporting Information. There are two options; option I when the phase shift is $\varphi = \pi$ and option II when the phase shift is $\varphi = 0$. The crossed tube is formed by a layer with an elliptical hole with length $l = \pi R$ and width $w = 2R$. There are two ways how the elliptical hole can be formed: either as one hole (Figure S2b, Supporting Information, option I) or as two "half" – holes with the same radius (Figure S2b, Supporting Information, option II). It is also crucial that both

layers fold not at once but with some delay in between because simultaneous folding shall result in the collision of folding sheets (Figure S3, Supporting Information). These calculations are based on the assumption that the size of layers does not change during the shape transformation. Our approach to fabricate shape-changing layers using hydrogels with a vertical gradient of swelling properties can be used to fabricate the above-described junctions.[12]

Nevertheless, swelling of such films results not only in vertical swelling, but also in lateral directions, i.e., the lateral size of the film changes. This means that the mathematical model requires re-adjustments by considering lateral swelling. We found empirically that the mathematical model described above involves multi-step printing and does not allow for simultaneous printing of sheets. In this case, the two sheets have to be printed individually to avoid mixing and fusion of the two structures during 3D printing, i.e., in the wet state. In other terms, the first sheet should be printed first and then dried completely, followed by the printing of the second sheet in the wet state that will result in the mixing or fusion of the structures at the overlap region. Moreover, 3D printing of the two sheets individually poses the challenge that the two structures should be kept manually in proximity during the immersion in aqueous media for proper overlapping of the structures and formation of the tight junction. Hence, the design was modified and adjusted to keep the two structures as close as possible to each other to avoid the separation of the two structures during the folding process. For this reason, the design is modified as follows; the design is composed of two individual rectangular sheets that are connected using a bridge-like structure (green rectangle in Figure 1a). One of the rectangles is composed of two identical elliptical geometries to form an elliptical hole (blue rectangle in Figure 1a). The other rectangle (yellow rectangle in Figure 1a) has precise sine wave functions that fit inside the hole of the first rectangular structure (blue rectangle in Figure 1a) to form the T-shaped bifurcation. The use of this approach allows the elimination of the need for multiple shape-changing hydrogels for synchronized folding and the use of adhesive or sacrificial materials to keep the tubes in proximity. In this way, the fusion and collision of the two structures can be avoided in the printing and folding process. In other terms, the wave functions were designed to create an overlap with the elliptical holes upon shape-transformation. Besides, keeping the two structures as close as possible to each other to avoid the fusion at the overlap region while 3D printing. That was possible by creating one wave function with a vertical shift of 2.19 units and horizontal shift of ± 1.64 units from the main axis while maintaining the other wave function normal with respect to the main axis of the drawing.

The ADA-Gel (1:2 *(w/w)*), which is a mixture of alginate dialdehyde 2.5% *(w/v)* and gelatin 5% *(w/v)*, was used as a biomaterial ink[9,30] for the 3D printing of the designed flat structures (Figure 1a). Further, the rheological properties of the ink were studied using oscillation experiments. First, an amplitude sweep at an oscillation frequency of 1 Hz was applied to determine the linear viscoelastic (LVE) limit. This is crucial for assessing the stability of the polymer solution under shear of various magnitudes. It was found that the LVE limit is at around $\gamma \approx 2\%$ strain. Furthermore, the solution showed a
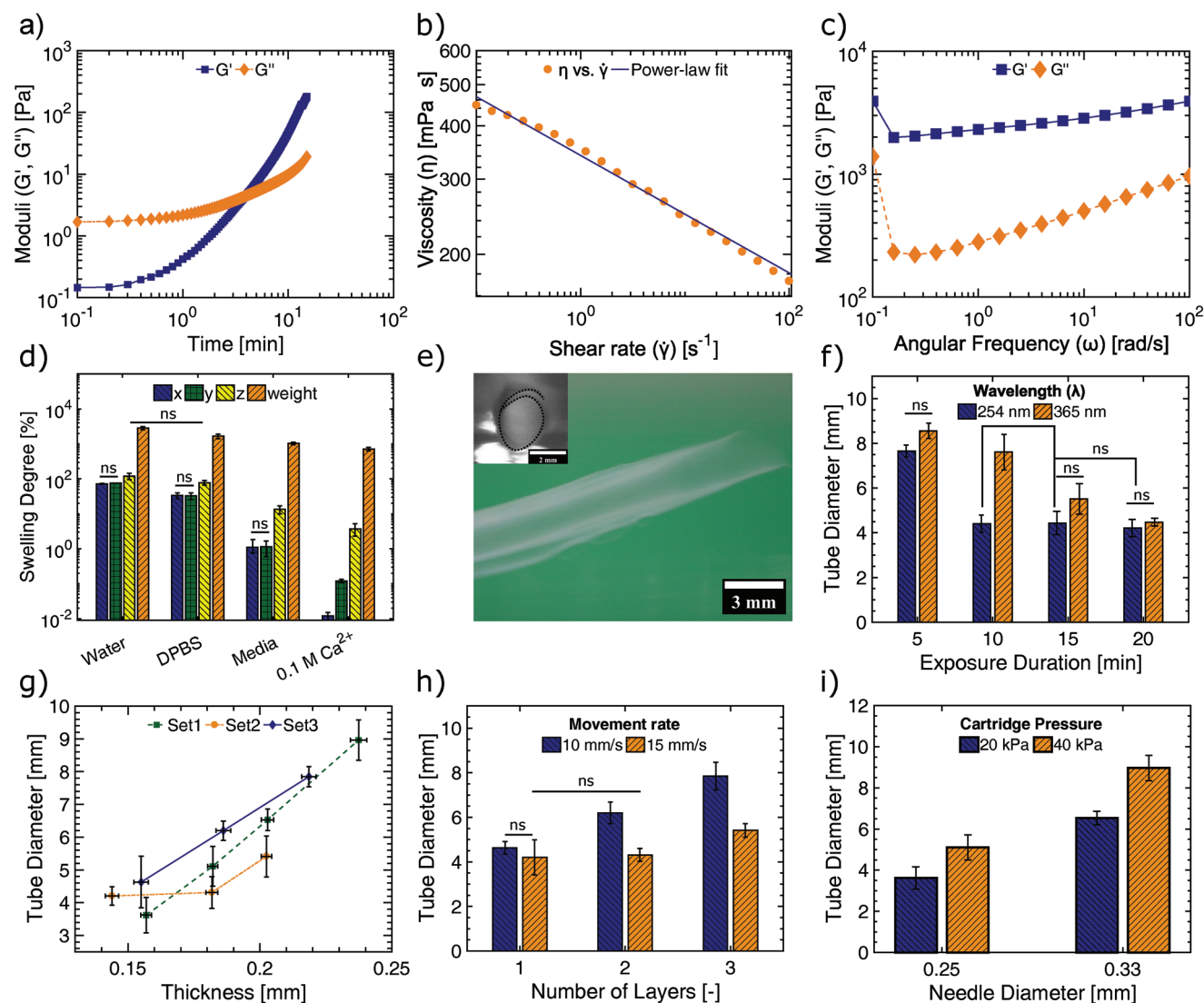
Figure 2. Rheological properties of the biomaterial ink and the effect of the 3D printing parameters on shape transformation: a) isothermal time sweep at room temperature showing the gelation point; b) viscosity versus shear rate indicating the shear thinning behavior; c) frequency sweep of the crosslinked and swelled hydrogel, d) the swelling behavior of the crosslinked hydrogel in different media, e) top and side views of the tube (insert scale 2 mm), and f–i) effect of exposure time, film thickness, number of layers, and needle inner-diameter on the final tube diameter. Data are shown as mean ± SD, $n = 6$ except for (d) $n = 3$, p-values are calculated using one-way ANOVA followed by multiple comparison test (post-hoc) with Bonferroni method ($p > 0.05$ is considered statistically not significant (ns)).

viscous-like behavior (loss modulus $G'' >$ storage modulus G') below $\gamma \approx 4\%$ strain (moduli intersection or crossover point) and showed a dominance of the storage modulus over the loss modulus at higher shear that is transition into the elastic-state. This experiment showed that there are physical networks of polymer, which relax at a low shear rate. Indeed, the shear rate in an oscillating experiment is linearly proportional to shear as $\dot{\gamma} = \gamma_0\,\omega \sin(\omega t)$ and the increase of the shear results in the increase of the shear rate and transition from flow to the viscoelastic regime (Figure S4a, Supporting Information). The frequency sweep of the ADA-Gel solution conducted at LVE (Figure S4b, Supporting Information) showed the domination of loss modulus ($G'' > G'$) at large frequencies. While G'' linearly decreases with the decrease of frequency until it reaches

the crossover point ($G' = G''$) at around 0.5 rad s⁻¹. The linear decrease in G'' with the decrease of frequency is an indication of the flow of the solution. On the other hand, both moduli rapidly increase with a further decrease in frequency below the crossover point, and storage modulus starts to dominate over loss modulus ($G' > G''$). The reason for this unexpected behavior, which cannot be assigned to any existing models of viscoelastic behavior, is the gelation of the solution with time – its viscoelastic properties changes with time. For this reason, the changes in the rheological properties of the solution with time were assessed using an oscillatory isothermal time sweep to determine the gelation point. **Figure 2**a shows that both storage and loss modulus increase with time and the gelation time was around 4 min, where G' and G'' intersect, and the

**ADVANCED
SCIENCE NEWS**

www.advancedsciencenews.com

**ADVANCED
MATERIALS
TECHNOLOGIES**

www.advmattechnol.de

G' becomes dominant over G''. Next, the flow behavior was assessed by steady-state rheology. It can be observed that the viscosity decreases with increasing shear rate and shear stress (Figure 2b), which indicates the shear-thinning behavior of the biomaterial. This behavior is due to that the hydrogen bonds between molecules tend to break with increasing shear rate. The shear-thinning behavior was quantified by the power-law fit of the viscosity η vs. shear rate $\dot{\gamma}$ that yielded power-law index $n = 0.86$. Thus, ADA-Gel is a viscoelastic ink, in which it forms a physical gel with the time – most probably – due to the formation of hydrogen bonds between the polymer molecules. Hence, applying a force during shearing breaks these hydrogen bonds, and the ink starts to flow.

Illumination with UV-light changes the mechanical properties of the polymer. Figure 2c shows the results of the frequency sweep, which depicts the effect of angular frequency on the rheological characteristics of the crosslinked hydrogel in its swelled state. It can be observed that the storage modulus is dominant over the loss modulus and the change in both moduli are nearly constant over the range of frequencies used. This indicates the absence of a relaxation process on a time scale of 0.01–10 s. Interestingly, both moduli increase at the last measured point (0.01 rad s^{-1}), which could be an indication of the formation of additional crosslinking points formed by hydrogen bonds. This also results in the gelation of the non-crosslinked parts of the hydrogel. Moreover, this indicates that the illumination of the 3D printed and dried ADA-Gel film induces intermolecular crosslinking of the polymer network, since some aromatic amino acids found in gelatin are sensitive to UV light of specific wavelengths.[31–33] As a result, it loses its ability to dissolve in aqueous conditions, and in turn, it gives rise to swelling (Figure 2d).
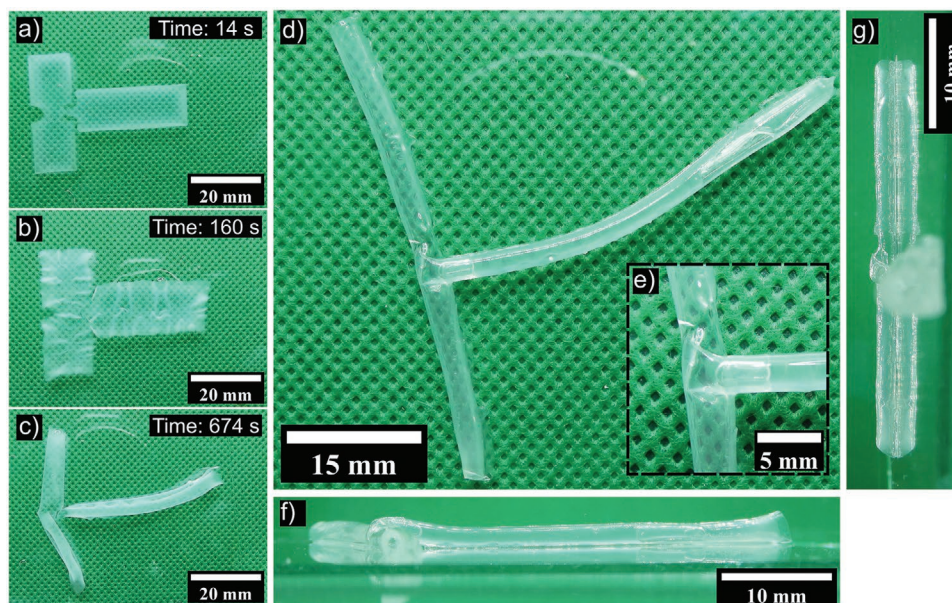
Additionally, we studied the effect of different aqueous media on the fabricated hydrogel film swelling properties. The selected aqueous media represents a wide range of solutions used in cell culture studies that has an effect on the swelling degree and in turn on tube diameter and stability of the hydrogel.[12] It was found that the crosslinked polymer swells extensively in pure water in all directions (Figure 2d). The swelling degree declines in the following order: pure water, DPBS, DMEM, and finally 0.1 M CaCl$_2$ solution. The decreased swelling degree observed in different buffer solutions can be explained by their higher ionic strength, which results in the shielding of charged polymer groups and suppression of electrostatic repulsions. The lowest swelling degree was observed in the CaCl$_2$ solution. Besides CaCl$_2$ high ionic strength, it also crosslinks alginate by chelation.[12,34] Thus far, it can be concluded that the swelling properties of the crosslinked polymer can be controlled by the ionic strength of the media.

We studied the effect of 3D printing parameters as well as the gelatin concentration on the thickness of the printed structures and, in turn, the final tube diameter (Figures 2e-i, S5, and S6, Supporting Information). It was found that the decrease in movement speed, increase in cartridge pressure, and increase in inner needle diameter resulted in an increase in the thickness of the 3D printed biomaterial ink (Figures S5 and S6, Supporting Information). This increase can be explained by the increased amount of the extruded ink through the needle with decreased movement speed, increased extrusion pressure, and increased needle diameter. Similarly, the increase in the gelatin

concentration of the solution increases the thickness of the 3D printed film in its dry state due to the increase in the gelatin dry content. The tube diameter tends to increase with the thickness of the dried 3D printed structures, which can be precisely controlled by varying the 3D printing parameters (Figure 2g–i). For instance, increasing needle diameter and the number of layers resulted in a direct increase in the final tube diameter (Figure 2h,i). It was also found that the tube diameter tends to decrease by increasing UV exposure time since the resulting tube diameter relies highly on the swelling degree. Further, the swelling degree is dependent on crosslinking density, in which longer exposure durations increase the crosslinking density, in turn decreasing swelling degree and correspondingly decreasing tube diameter, as shown in Figures 2f and S7, Supporting Information.[12] Overall, the tube diameter of samples crosslinked under UV-light of wavelength 365 nm is larger than for samples crosslinked under 254 nm. This is due to the fact that certain aromatic amino acids found in gelatin, such as tyrosine and phenylalanine, have more substantial absorbance to UV light of the wavelength of 254 nm.[31–33] As a result, this increases the crosslinking density of the biomaterial ink. These studies allowed finding the optimal 3D printing parameters for the programmed 4D biofabrication of the designed structure (Figure 1a) to form T-shaped bifurcations. In conclusion, a 3D printing speed of 15 mm s^{-1}, printing pressure of 20 kPa, needle size of 25 G (Ø of 0.25 mm), and layer count of 3 was chosen for the 3D printing of T-shaped structures since they have shown a compromise between printing time, thickness, and targeted range of tube diameters of less than 6 mm (Table 1). Finally, the side and transverse view of the obtained

Table 1. The optimized 3D printing and ultraviolet (UV) crosslinking parameters that were used for the biofabrication of the T-junction.

Parameters	3D printing biomaterial ink	
Solvent		
	Solvent system	DPBS
	ADA concentration	2.5% (w/v)
	Gel concentration	5% (w/v)
Set-up		
	Layer height	0.1 [mm]
	Initial height	0.1 [mm]
	Number of Layers	3
	Cartridge pressure	20 [kPa]
	Needle size	25 G
	Needle length	25.4 [mm]
	Movement speed	15 [mm s^{-1}]
	Glass slide	80 × 80 [mm]
3D Printing conditions		
	Temperature	30 °C
	Humidity	Ambient
Crosslinking		
	Type	UVC
	Wavelength	254 [nm]
	Exposure time	20 [min]
	Distance	17 [mm]

**ADVANCED
SCIENCE NEWS**

www.advancedsciencenews.com

**ADVANCED
MATERIALS
TECHNOLOGIES**

www.advmattechnol.de

Figure 3. Self-folding of the 3D printed structures and the formation of T-junction in pure water: a) the initial dried and UV crosslinked hydrogel directly after water addition, b) the swelling and detachment of sample from the substrate at a time frame of 160 s, c) the formation and folding of the T-junction at a time frame of 674 s, d) the final T-junction after the removal of water and slight drying, e) a zoomed view at the junction area, f), and g) side views of the structure.

tube T-junction segment is shown in Figure 2e, where it can be observed that it has a spiral-like structure with approximately one and a half folds and an outer diameter of around 2.5 mm as well as an inner diameter of roughly 2 mm. Thus, the 3D printed, dried, and photo-crosslinked structures were able to roll, swell, and form tubular structures upon immersion in aqueous media.

The 3D printed and crosslinked ADA-Gel 1:2 (w/w) plain T-junction structures (geometry shown in Figure 1a) undergo controlled shape-transformation due to swelling of the polymer and, in turn, form a hollow tubular T-junction (**Figure 3**a–g, Videos S8 and S9, Supporting Information). It starts with the unfolded dried and UV-crosslinked thin film of an average thickness of 0.2 mm (Figure 3a), followed by the addition of pure water and the diffusion of water from all directions within the ADA-Gel structure. Next, the swelling and detachment of the sample after around two minutes is initiated (Figure 3b). Hence, the detachment of the structure starts from the sides, which are relatively thin, and progress with the detachment of the middle part, which is relatively thick. This will further help in the actuation process and the formation of a tubular structure. Finally, the self-actuation and complete folding of the sample into a T-junction of a tubular structure with an average diameter of 5 ± 1 mm after around 11 min is shown in Figure 3c. After the shape transformation was achieved, water was removed entirely from around the sample, and the tubular structure was also emptied of water and let dry for further investigations (Figure 3d). The T-junction obtained after water removal and drying has an average tube diameter of 3 ± 0.3 mm, representing a decrease in tube diameter of 66% from the wet state, which led to the formation of a tightly closed tubular structure (Figure 3d–g). The folding direction of the T-junction along the long side of the rectangular structures

(Figure 1d) was precisely controlled by fixing the aspect ratio (width to length) as well as the thickness of the films.[35] In particular, an aspect ratio of 3 between the width and length of the individual structures (shown in blue and yellow in Figure 1a) as well as an average thickness of 0.2 mm allowed for the transversal folding into tubular structures after the addition of water Figure 3c. Moreover, the small gap distance of 1 mm and the bridging structure between the two rectangles as well as the precisely designed geometry (wave functions and ellipses in Figure 1a) – as theoretically described earlier – support the tight formation of the T-junction upon the removal of water from the sample (Figure 3d–g).

The self-folded and dried T-junction samples were perfused using a red aqueous solution to simulate blood flow through a vascular bifurcation and to check that the T-junction was hermetically sealed and no leakages were present. **Figure 4**a–e indicates that the aqueous solution easily passed through the structure with minimal leakages (Videos S10 and S11, Supporting Information), which shows that the T-junction is hermetically sealed and presents a promising candidate for vascular tissue engineering applications. Additionally, it shows that the final T-junction after perfusion with a red solution can hold its shape and the perfused solution within its structure. Additionally, the perfused aqueous solution has an average flow velocity of 0.04 m s^{-1} and a maximum flow velocity of 0.11 m s^{-1} (0.78 mL s^{-1} in 3 mm diameter bifurcated structure), which is comparable to blood flow velocity in native blood vessels with comparable diameters to the structure fabricated in this study.[36] For instance, Klarhöfer et al.,[21] measured the arterial blood flow in the human index. They have reported a maximum blood flow velocity of 0.19 m s^{-1} through blood vessels in the diameter range (0.8 – 1.8 mm) and significantly lower blood velocity in veins with a maximum velocity of 0.07 m s^{-1}.[29] This
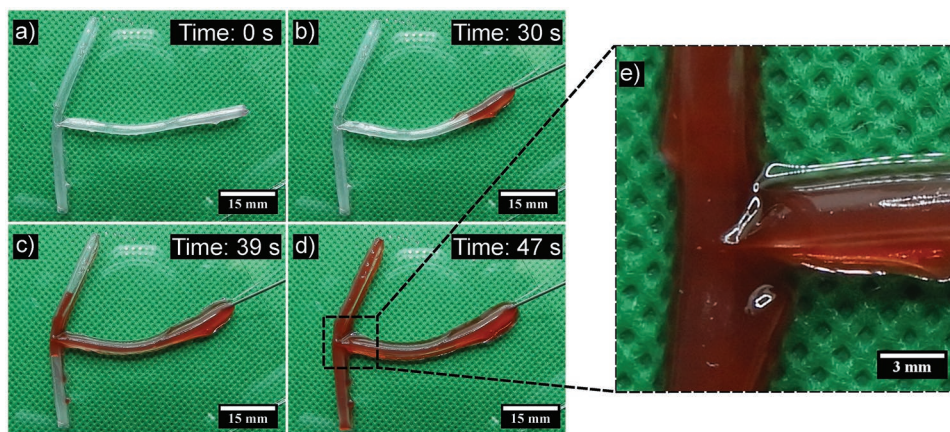
Figure 4. Red aqueous solution perfusion through the final T-junction, were a) the dried and emptied T-junction at time frame 0 s, b) the start of the perfusion process, in which the dye passed through the first structure (30 s), c) the dye perfusion through the junction area (39 s), d) the perfusion through the whole structure (47 s), and e) a zoomed view at the junction area.

shows that the measured flow velocity through the prepared T-junction is comparable to native blood vessels of similar diameter.

Finally, we have studied the behavior of HUVECs seeded on the inner surface of the formed T-junctions. DAPI – F-actin staining of HUVECs cultured on the inner surface of the self-folded T-junctions showed outstanding cells adhesion and growth properties across the structure as well as excellent cell viability measured using live/dead assay (**Figure 5**a–e). Hence, cells were able to form a complete monolayer with a coverage degree of 87 ± 7% (Figure 5a,b). In addition, cells showed excellent cell proliferation with an alamarBlue reduction of 35 ± 4% and 31 ± 7% on days 4 and 7, respectively, with statistically no significant difference between the days of incubation (Figure 5e). Further, the samples showed an excellent cell

viability of 98.5 ± 0.7% and 98.3 ± 1.3% on days 4 and 7, with no significant difference between days of incubation as well (Figure 5e). Previously, Ruther et al. assessed the viability of cocultured fibroblast and HUVEC cells cultured on ADA-Gel vessel-like structures for 3 weeks and reported that the viability of cells was doubled with each proceeding week of incubation and the cell viability was around 98%.[9] In addition to that, it was concluded that HUVEC cocultured fibroblasts were able to migrate considerably through the fabricated ADA-Gel scaffold.[9] This can also be observed in ADA-Gel samples fabricated in this study, as the inner surface of the structure was fully covered within one week of cell culture (Figure 5a,b). In conclusion, ADA-Gel is a promising candidate for HUVECs adhesion and growth and shows very high cell viability on days 4 and 7 of culture.
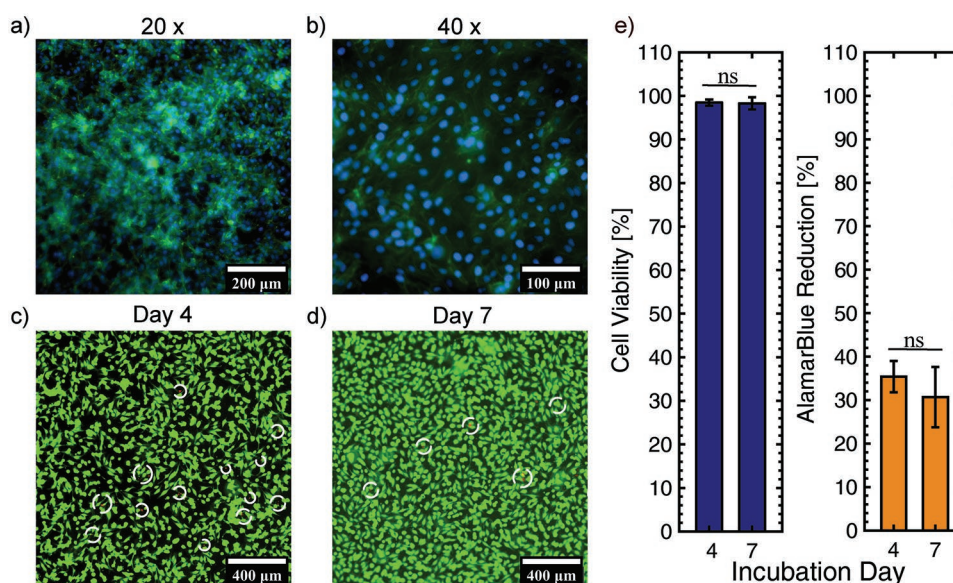
Figure 5. Cell culture results showing DAPI – F-actin staining of the nucleus (blue) and cell body (green) of ADA-Gel at different magnifications with a) 10x and b) 40x, live/dead assay with live cells shown in green and dead cells shown in red (white circles) at day c) 4 and d) 7, as well e) showing the average cell viability and proliferation at the days of incubation. Data are presented as mean ± SD, $n = 3$, p-values are calculated using one-way ANOVA followed by a multiple comparison test with the Bonferroni method ($p > 0.05$ is considered statistically not significant (ns)).

**ADVANCED
SCIENCE NEWS**

www.advancedsciencenews.com

**ADVANCED
MATERIALS
TECHNOLOGIES**

www.advmattechnol.de

3. Conclusion

In this paper, we, for the first time, demonstrated the possibility of the fabrication of elements of vascular networks such as T-junctions by controlled shape transformation of 3D printed hydrogel structures fabricated using ADA-Gel. A mathematical model is proposed, which allows calculation of the shape of the 3D printed object to achieve the desired shape-transformation, and partially realized it by 3D printing of biocompatible/biodegradable oxidized alginate-gelatin ink. It was also demonstrated that the formation of hollow tubular structures in the form of T-junctions in scalable diameters is possible using hydrogel-based shape-changing layers with a vertical gradient of swelling properties. This can be achieved by the precise control of the 3D printing parameters; layer number, needle diameter, printing speed and pressure, hydrogel concentration, as well as the crosslinking parameters including wavelength, intensity, and exposure time. Our approach allows the fabrication of tube-like structures with diameters ranging from 2 to 15 mm by adjusting the 3D printing parameters. Additionally, smaller diameters can be achieved by scaling down the size of the geometry of the 3D printing structure. The achieved diameters are comparable to the native blood vessels (small $\varnothing < 6$ to large $\varnothing > 8$ mm). This paves the way for the fabrication of vascular grafts of different geometries made from a wide range of swellable biomaterials with tunable mechanical and biological properties. Finally, the fabricated T-junction allowed exceptional HUVECs growth and adhesion by forming a complete cellular monolayer. Additionally, HUVECs showed high average cell viability (98%) and proliferation (33%) on the printed structures. We believe that the proposed concept of controlled shape transformation will offer new solutions for the fabrication of artificial blood vessels or vascular grafts.

4. Experimental Section

Materials: Sodium alginate (from brown algae, VIVAPHARM PH163S2 Alginate – JRS PHARMA GmbH & Co. KG, Rosenberg, Germany), Human Vascular Endothelial Cell (HUVEC) Medium (InSCREENeX GmbH, Braunschweig, Germany), Formaldehyde solution 37% (CH₂O) (≥37%, for synthesis – Carl Roth GmbH + Co. KG, Karlsruhe, Germany), Dialysis Membrane tubing (Spectra/Por, Molecular porous membrane tubing, Standard RC tubing, MWCO: 6–8 kDa – Spectrum Laboratories, Inc., Rancho Dominguez, California, USA). Gelatin from porcine skin (Type A, BioReagent), Sodium metaperiodate (NaIO₄), Ethylene glycol (Anhydrous 99.8%,), Dulbecco's Phosphate Buffered Saline (DPBS) (Modified, without calcium chloride and magnesium chloride), Triton X-100 ($\overline{M}_n$ = 625 g mol⁻¹, for molecular biology), Ethanol absolute (ACS grade reagent, ≥99.5% (GC)), Collagen (from rat tail tendon), and Calcium chloride dihydrate (CaCl₂·2H₂O) were purchased from Sigma-Aldrich Co Ltd., St. Louis, Missouri, USA. 4′,6-diamidino-2-phenylindole (DAPI) (C₁₆H₁₇Cl₂N₅, Dihydrochloride), Phalloidin Daylight 488 conjugated 300 (300 units mL⁻¹), alamarBlue Reagent (Cell Viability Reagent), Calcein AM (C₄₆H₄₆N₂O₂₃), and Ethidium Homodimer-1 (EthD-1) (C₄₆H₅₀Cl₄N₈) were purchased from Thermo Fisher Scientific Inc., Waltham, Massachusetts, USA.

Synthesis of Alginate Di-Aldehyde (ADA): Alginate di-aldehyde (ADA), also known as oxidized alginate, was synthesized as described by Sarker et al. with slight adaptations.[37] Shortly, an alginate 20% (w/v) suspension was prepared by mixing alginate with ethanol under constant stirring. Next, sodium metaperiodate (NaIO₄) was dissolved in ultrapure water and mixed thoroughly. After that, NaIO₄ solution was added stepwise to the alginate

suspension under increased stirring for 6 h to ensure complete mixing of the two solutions for successful oxidation. The previous steps were conducted at room temperature and under complete dark conditions. After 6 h, the reaction was quenched with ethylene glycol for 30 min to terminate the oxidation process. Finally, ADA was dialyzed against ultrapure water for 4 days, frozen at −20 °C, and freeze-dried for later use.

Preparation of ADA-Gel Solution: The ADA-Gel solution was prepared as described by Sarker et al.[37] At first, 5% (w/v) alginate di-aldehyde (ADA) solution was prepared by dissolving ADA in DPBS at room temperature and a constant stirring of 70 rpm until completely dissolved. Meanwhile, 10% (w/v) gelatin (Gel) solution was prepared by dissolving in DPBS at a constant stirring of 350 rpm and using a heated water bath of 37 °C until thoroughly dissolved. Next, equal volumes (1:1 (v/v)) of both solutions were blended and constantly stirred at 150 rpm for 10 min in a water bath of 37 °C. The final solution contains 2.5% (w/v) ADA and 5% (w/v) of Gel resulting in the ratio 1:2 (w/w) of ADA-Gel solution.

Rheological Investigations: The modular rheometer (Anton Paar MCR 702 MultiDrive Rheometer, Anton Paar GmbH, Graz, Austria) was used to study the rheological properties of ADA-Gel solutions and hydrogels. Therefore, a frequency sweep test was done with an initial angular frequency (ω) of 100 rad s⁻¹ and a final angular frequency (ω) of 0.1 rad s⁻¹ with 16 data points, an interval of 12.9 min, temperature of 30 °C, and 2% strain. An oscillatory isothermal time sweep was also conducted at a frequency of 1 Hz, temperature of 25 °C, and shear strain of 10% for 15 min. This test was done to study the rheological changes of the solution with time. Additionally, an amplitude sweep was operated at a frequency of 1 Hz and a shear strain range from 0.01% to 100%. For these measurements, a parallel plate geometry with a measuring diameter ($\varnothing$) of 25 mm and a gap distance of 0.6 mm in oscillatory mode was used. A shear-rate ramp test was also done to assess the flow behavior of the biomaterial ink. The tests were done with an initial shear rate ($\dot{\gamma}$) of 0.1 s⁻¹ and a final shear rate of 100 s⁻¹ for 30 s at 30 °C for 21 data points. Moreover, the flow experiment was operated using a cone-plate geometry with cone angle (φ_0) of 0.93°, measuring diameter ($\varnothing$) of 59.97 mm, and gap distance of 0.12 mm. The flow (power-law) index (n) was found using the power-law model, which is a model that describes the shear-thinning behavior of polymer solutions from the viscosity (η) vs. shear rate ($\dot{\gamma}$) plot obtained from flow experiments. For this, the power-law (i.e., the linear) region of the graph was fitted using the following equation: $\eta = \kappa \dot{\gamma}^{n-1}$.

Printing Parameters: In this study, the multi-headed bioprinter (3DDiscovery Evolution – BioSafety Cabinet Class II, 3D bioprinter, regenHU Ltd., Villaz-Saint-Pierre, Switzerland) with the integrated pneumatic pressure extruder DD135-H was used for the 3D printing of ADA-Gel. Different hydrogel concentrations, needle sizes, movement speeds, and cartridge pressures were tested for optimized 3D printing of the hydrogel. The 3D printing temperature of the hydrogel was regulated by setting the temperature of the syringe holder to 30 °C using the integrated Jumo dTRON 316 temperature regulator. Next, the solutions were loaded into a 5 mL hydrogel bioprinting cartridge with a piston and a pneumatic pressure adapter connected by a tube to the air pressure module. The printing solution was left at the 3D printing temperature for at least 30 min to ensure homogeneous distribution of the heat throughout the solution before starting the 3D printing process and ensuring the solution's relaxation.

To study the effect of the 3D printing parameters on the sample thickness and, in turn, on the resulting tube diameter, variations in the printing pressure, movement speed, layer count, and needle size were investigated. Additionally, two different concentrations of ADA-Gel were studied to determine the optimal 3D printing parameters. After examining the optimal 3D printing parameters (summarized in Table 1), the T-Junction was 3D printed on a custom-made glass slide of size 80 × 80 mm. The T-junction CAD model was sliced with a concentric infill structure with a gap size of 0.16 mm and an angle of 45° using BioCAD (RegenHU Ltd., Villaz-Saint-Pierre, Switzerland). The design has two structures with a cuboidal shape of dimension 45 × 16 × 0.2 mm (*L* × *W* × *H*). Additionally, one of the structures has two symmetrical ellipses of a major axis (*x*-axis) of a radius of 5 mm and a minor axis (*y*-axis) of a radius of 3.5 mm. Furthermore, the second structure has at one end a single sine

© 2022 The Authors. Advanced Materials Technologies published by Wiley-VCH GmbH

wave function, $\left(f(x) = A\sin\left(\frac{\omega}{T}x \pm \varphi\right) \pm D \right)$ of amplitude (A) of 1.6 mm and wavelength (T) of 8 mm (Figure 1a). Besides that, it has a second sine wave function of A of −1.6 mm and T of 8 mm with a phase-shift (φ) of 1.64 mm from one edge and −1.64 mm from the other edge with a vertical shift (D) of 2.19 mm. The third structure is cuboidal with dimensions of $8 \times 4 \times 0.2$ mm that functions as a bridge between the other two structures.

UV Crosslinking: For the determination of the optimal crosslinking conditions for the proper self-folding of the samples, the UV Lamps VL-215.C (λ: 254 nm) and VL-215.L (λ: 365 nm) (UV Lamp, 2 × 15 W Tube Vilber Lourmat, Marne-la-Vallée, France) were used. Thus, the 3D printed samples were crosslinked at different exposure durations using two wavelengths (254 and 365 nm) at a 17 mm distance from the lamp.

Thickness and Tube Diameter Measurements: For measuring the overall thickness of the 3D printed samples, the Nikon Eclipse Ti2 inverted microscope with an integrated DS-Qi2 Nikon digital camera was used (Nikon Instruments Inc., Tokyo, Japan). The samples were left to thoroughly dry out at room temperature for overnight before measuring the thickness to account only for the thickness of the material. For this, the z- series acquisition mode (z movement option) of the NIS-elements 5.21.00 LO software was used to get an approximation of the thickness of the samples. Additionally, 4x objective lens and phase contrast condenser PhL were used to capture the top and the bottom of the sample by changing image focus and getting the range of in-focus of the sample for the approximation of the thickness. Moreover, the measurement was done by taking a set of measurements in three different regions along the length of the sample and calculating the mean and standard deviation for each sample. For the measurement of the tube outer diameter, three sets of two measurements were done along the length of the samples using ImageJ. The images were taken using the Nikon Coolpix B700 Camera (Nikon Corporation, Tokyo, Japan).

Swelling Studies: The swelling properties of ADA-Gel in different aqueous solutions were investigated by calculating the swelling ratio between the swollen or the hydrated state and the dried state of the hydrogel using Equation 1. Thus, the weight and the dimensional expansion of the hydrogel in all directions were measured at both the hydrated and dried state. For this, 10 × 10 mm squares were printed on a glass slide and left to dry overnight. Next, the dried samples were crosslinked using UV light (λ: 254 nm) for 5 min at a distance of 17 mm from the lamp. Finally, the swelling degree was examined in ultrapure water, DPBS, HUVEC cell culture media, and at 0.1 M calcium chloride solution and let immersed for 30 min to ensure complete hydration of the samples.

$$\text{Swelling Degree}(\%) = \frac{W_s - W_d}{W_d} \times 100\% \qquad (1)$$

where W_s and W_d are the weight or the dimension in the swelling and dried state, respectively.

Cell culture studies: Human umbilical vein endothelial cells (HUVECs) (passage number < 7) were seeded on the T-junction samples. The T-junction samples were 3D printed and prepared under aseptic conditions. The 3D printed samples were let dry for at least overnight and then crosslinked using a 254 nm UV light for 15 min at a 17 mm distance from the UV light source. Before cell culture, the samples were coated with 200 µL collagen solution (0.2% (w/v) in acetic acid) to enhance cell adhesion to the samples. The excess collagen solution was removed to form a thin coating and then let dry for 15 min. Afterward, the samples were seeded with 0.2×10^6 cells cm^{-2} cell density and incubated for 5 h to ensure complete adhesion of the cells. Finally, the samples were folded in autoclaved tap water, followed by water removal and the addition of a human vascular endothelial cell (HUVEC) culture medium. Several media changes were done on days 1, 3, and 5 until the high confluency of cells was reached (>90%).

Actin Filament (F-Action) and Nucleus Staining: The growth and adhesion of HUVECs cultured on the T-junction samples were evaluated by visualizing the actin filaments and cell nuclei by staining the nucleus with 4′,6-diamidino-2-phenylindole (DAPI), and F-actin with Phalloidin Daylight 488 conjugated 300 at day 5. The final staining solution contains; 500 µL DAPI with a concentration of 1% (w/v), 10 mL DPBS, and 250 µL Phalloidin Daylight 488 with 200 units mL^{-1} dissolved in methanol. First, the cell culture media was aspirated, and then the samples were washed twice with DPBS. Subsequently, the cells were fixed with formaldehyde 3.7% (1 mL 37% formaldehyde in 9 mL DPBS) for 15 min and washed two times with DPBS to remove the fixative solution. Next, the cell membrane was permeabilized by 0.1% Triton 100 X solution (10 µL in 10 mL DPBS) for 5 min at ambient conditions and washed twice with DPBS. Finally, the staining solution was added to cover the samples entirely for 30 min at room temperature, and then the staining solution was aspirated and washed two times with DPBS. In the end, the samples were kept in DPBS and covered with aluminum foil before visualizing them under the Nikon Ti2 microscope.

Cell Proliferation and Live/Dead Assays: The intracellular reduction of alamarBlue and the hydrolysis of Calcein AM were used to quantify the metabolic activity (proliferation) and cell viability of HUVECs seeded on ADA-Gel substrates, respectively, for days 4 and 7. For this, the dried and UV-crosslinked ADA-Gel samples were prepared on a 24-well cell culture plate and seeded with a cell density of 200 000 cells cm^{-2}. Next, the samples were covered with HUVEC cell culture media and incubated for 5 h. Before cell culture, the samples were coated with a thin film of 0.2% (w/v) collagen solution and let dry for 15 min to enhance cell adhesion to the substrates. A total number of 5 replicates were used in this quantification for each study day.

To assess cell proliferation, 10% (v/v) of the alamarBlue reagent in HUVEC cell culture media was added to cover the samples thoroughly. Next, the samples were incubated for 90 min with gentle shaking or rocking of the well plate in all directions every 30 min. This step will ensure the complete distribution of the reagent and avoid gradient formation. After incubation, the reacted media were taken from each well into aliquots and kept on ice under dark conditions to stop the reaction. Next, three sets of 100 µL of the reacted media were pipetted from each aliquot into a 96-well cell culture plate. Afterward, fluorescence was measured using the plate reader (TriStar^2 S LB 942 Multimode Microplate Reader, Berthold Technologies GmbH & Co.KG, Germany) at 535 nm excitation and 600 nm of emission wavelength. Negative control was prepared using the unreacted alamarBlue (10% in culture media), and positive control was prepared using 10% (v/v) of the 100% reduced alamarBlue in sterile deionized water. The negative and positive solutions were used to calculate the percentage of alamarBlue reduction.

After that, a staining solution of 3.6 µL of Calcein AM, 4 µL of ethidium homodimer-1, and 2 mL of DPBS was prepared to determine cell viability. Calcein AM was used to stain live intact cells, which is hydrolyzed by intracellular metabolic esterase of living cells and retained within their cytoplasm, producing the fluorescently detected green Calcein. Whereas the cell-membrane-impermeant ethidium homodimer-1 was used to stain dead cells, in which it binds to the nucleic acid of dead cells emitting red fluorescence. For this, the prepared solution was added to sufficiently cover each well and incubated at room temperature for 30 min in dark conditions before imaging. Finally, the samples were visualized under the Nikon Ti2 microscope, the number of dead and live cells were counted from several images, and the viability was calculated on days 4 and 7.

Statistical Analysis: Statistical analysis was done to assess the statistical significance of the tested samples and groups. Multiple comparisons of one-way analysis of variance (one-way ANOVA) followed by the multiple comparison test of the critical-value type of the Bonferroni method were performed using the Statistics and Machine Learning Toolbox of Matlab R2022a. The comparisons were considered significant, with *$p < 0.05$, whereas with $p > 0.05$ is considered not significant (ns). If not elsewhere stated, all results were significantly different within each group and between different groups of each experiment.

Supporting Information

Supporting Information is available from the Wiley Online Library or from the author.

[1] World Health Organization (WHO), Cardiovascular diseases (CVDs), https://www.who.int/news-room/fact-sheets/detail/cardiovascular-diseases-(cvds)#.X-xxgQtjP9E.link (accessed: June 2021).

[2] E. Wilkins, L. Wilson, K. Wickramasinghe, P. Bhatnagar, J. Leal, R. Luengo-Fernandez, R. Burns, M. Rayner, N. Townsend, in *European Cardiovascular Disease Statistics* (Ed: S. Løgstrup), European Heart Network, Brussels **2017**.

[3] C. D. Mathers, D. Loncar, *PLoS Med.* **2006**, *3*, e442.

[4] M. Rabionet, A. J. Guerra, T. Puig, J. Ciurana, *Proc. CIRP* **2018**, *68*, 352.

[5] P. Abdulhannan, D. A. Russell, S. Homer-Vanniasinkam, *Br. Med. Bull.* **2012**, *104*, 21.

[6] L. Xu, M. Varkey, A. Jorgensen, J. Ju, Q. Jin, J. H. Park, Y. Fu, G. Zhang, D. Ke, W. Zhao, R. Hou, A. Atala, *Biofabrication* **2020**, *12*, 045012.

[7] Q. Zhao, J. Wang, H. Cui, H. Chen, Y. Wang, X. Du, *Adv. Funct. Mater.* **2018**, *28*, 1801027.

[8] G. Soldani, P. Losi, M. Bernabei, S. Burchielli, D. Chiappino, S. Kull, E. Briganti, D. Spiller, *Biomaterials* **2010**, *31*, 2592.

[9] F. Ruther, T. Distler, A. R. Boccaccini, R. Detsch, *J. Mater. Sci.: Mater. Med.* **2018**, *30*, 8.

[10] Q. Zhang, È. Bosch-Rué, R. A. Pérez, G. A. Truskey, *APL Bioeng.* **2021**, *5*, 021507.

[11] Y. S. Zhang, F. Davoudi, P. Walch, A. Manbachi, X. Luo, V. Dell'Erba, A. K. Miri, H. Albadawi, A. Arneri, X. Li, X. Wang, M. R. Dokmeci, A. Khademhosseini, R. Oklu, *Lab Chip* **2016**, *16*, 4097.

[12] A. Kirillova, R. Maxson, G. Stoychev, C. T. Gomillion, L. Ionov, *Adv. Mater.* **2017**, *29*, 1703443.

[13] J. Hinton Thomas, Q. Jallerat, N. Palchesko Rachelle, H. Park Joon, S. Grodzicki Martin, H.-J. Shue, H. Ramadan Mohamed, R. Hudson Andrew, W. Feinberg Adam, *Sci. Adv.* **2015**, *1*, e1500758.

[14] W. Jia, P. S. Gungor-Ozkerim, Y. S. Zhang, K. Yue, K. Zhu, W. Liu, Q. Pi, B. Byambaa, M. R. Dokmeci, S. R. Shin, A. Khademhosseini, *Biomaterials* **2016**, *106*, 58.

[15] K. Christensen, C. Xu, W. Chai, Z. Zhang, J. Fu, Y. Huang, *Biotechnol. Bioeng.* **2015**, *112*, 1047.

[16] B. Grigoryan, J. Paulsen Samantha, C. Corbett Daniel, W. Sazer Daniel, L. Fortin Chelsea, J. Zaita Alexander, T. Greenfield Paul, J. Calafat Nicholas, P. Gounley John, H. Ta Anderson, F. Johansson, A. Randles, E. Rosenkrantz Jessica, D. Louis-Rosenberg Jesse, A. Galie Peter, R. Stevens Kelly, S. Miller Jordan, *Science* **2019**, *364*, 458.

[17] X. Han, J. Courseaus, J. Khamassi, N. Nottrodt, S. Engelhardt, F. Jacobsen, C. Bierwisch, W. Meyer, T. Walter, J. Weisser, R. Jaeger, R. Bibb, R. Harris, *Int. J. Bioprint.* **2018**, *4*, 2.

[18] E. Pektok, B. Nottelet, J.-C. Tille, R. Gurny, A. Kalangos, M. Moeller, B. H. Walpoth, *Circulation* **2008**, *118*, 2563.

[19] S. de Valence, J.-C. Tille, D. Mugnai, W. Mrowczynski, R. Gurny, M. Möller, B. H. Walpoth, *Biomaterials* **2012**, *33*, 38.

[20] S. Cheng, Y. Jin, N. Wang, F. Cao, W. Zhang, W. Bai, W. Zheng, X. Jiang, *Adv. Mater.* **2017**, *29*, 1700171.

[21] L. Ionov, *Adv. Healthcare Mater.* **2018**, *7*, 1800412.

[22] V. Stroganov, J. Pant, G. Stoychev, A. Janke, D. Jehnichen, A. Fery, H. Handa, L. Ionov, *Adv. Funct. Mater.* **2018**, *28*, 1706248.

[23] W. Zhou, Z. Qiao, E. Nazarzadeh Zare, J. Huang, X. Zheng, X. Sun, M. Shao, H. Wang, X. Wang, D. Chen, J. Zheng, S. Fang, Y. M. Li, X. Zhang, L. Yang, P. Makvandi, A. Wu, *J. Med. Chem.* **2020**, *63*, 8003.

[24] C. Cui, D.-O. Kim, M. Y. Pack, B. Han, L. Han, Y. Sun, L.-H. Han, *Biofabrication* **2020**, *12*, 045018.

[25] L. Zhang, Y. Xiang, H. Zhang, L. Cheng, X. Mao, N. An, L. Zhang, J. Zhou, L. Deng, Y. Zhang, X. Sun, H. A. Santos, W. Cui, *Adv. Sci.* **2020**, *7*, 1903553.

[26] S. Zakharchenko, E. Sperling, L. Ionov, *Biomacromolecules* **2011**, *12*, 2211.

[27] A. Rath, S. Mathesan, P. Ghosh, *Soft Matter* **2016**, *12*, 9210.

[28] S. Mathesan, A. Rath, P. Ghosh, *J. Phys. Chem. B* **2017**, *121*, 4273.

[29] M. Klarhöfer, B. Csapo, C. Balassy, J. C. Szeles, E. Moser, *Magn. Reson. Med.* **2001**, *45*, 716.

[30] T. Distler, A. A. Solisito, D. Schneidereit, O. Friedrich, R. Detsch, A. R. Boccaccini, *Biofabrication* **2020**, *12*, 045005.

[31] S. Maharana, P. K. Misra, *J. Phys. Chem. B* **2018**, *122*, 5161.

[32] A. R. Goldfarb, L. J. Saidel, *Science* **1951**, *114*, 156.

[33] C. Hazra, T. Samanta, V. Mahalingam, *J. Mater. Chem. C* **2014**, *2*, 10157.

[34] L. R. Shivakumara, T. Demappa, *Turk. J. Pharm. Sci.* **2019**, *16*, 252.

[35] G. Stoychev, S. Zakharchenko, S. Turcaud, J. W. C. Dunlop, L. Ionov, *ACS Nano* **2012**, *6*, 3925.

[36] C. L. Carter, *J. Cardiopulm. Rehabil. Prev.* **1989**, 9.

[37] B. Sarker, D. G. Papageorgiou, R. Silva, T. Zehnder, F. Gul-E-Noor, M. Bertmer, J. Kaschta, K. Chrissafis, R. Detsch, A. R. Boccaccini, *J. Mater. Chem. B* **2014**, *2*, 1470.